INFORMATION THEORETIC DISCREPANCY BASED ITERATIVE RECONSTRUCTION FOR TRANSMISSION TOMOGRAPHY

Kwang Eun Jang, Younghun Sung, Jongha Lee, Kangeui Lee, Jae Hak Lee, Seongdeok Lee*

Advanced Media Laboratory, Samsung Advanced Institute of Technology (SAIT)
San 14, Nongseo Dong, Giheung Gu, Yongin, Gyeonggi, Republic of Korea

ABSTRACT

The monochromatic approximation, which postulates that a source emits monochromatic radiation, has been widely used in the transmission tomography. However, due to the ignorance of energy dependency, image degradations such as beam hardening artifact are often occurred. In this paper, we present novel reconstruction algorithms to reflect the exact polychromatic model. Departing from the conventional algebraic and statistical reconstructions, the generalized information theoretic discrepancy (GID) is employed as the new data fidelity metric. By using the particular features of the GID, the cost function is derived in terms of imaginary variables, which incorporates energy dependency and leads to a tractable optimization problem even without the monochromatic approximation. In preliminary experiments with a simulated dual energy CT and a real experimental tomosynthesis, the proposed information theoretic discrepancy based iterative reconstruction (IDIR) algorithm showed superior performances over conventional reconstruction schemes.

Index Terms— Iterative reconstruction, tomographic reconstruction, dual energy CT, breast tomosynthesis

1. INTRODUCTION

Recently, the iterative reconstruction has obtained increasing interest for transmission tomography. As the speed and capacity of computing devices are improved significantly, it has been successfully installed in modern commercial computed tomography (CT) scanners. Since the iterative reconstruction method incorporates a sophisticate data acquisition model and a variety of regularization techniques, it often outperforms a conventional filtered backprojection method.

Iterative reconstruction algorithms are obtained by minimizing an object function, including the distance between measurements and synthetic data and a regularization term, and can be classified into two categories: algebraic and statistical reconstructions, according to the way to determine the data fidelity term. In both approaches, the monochromatic approximation is frequently employed, which postulates that the X-ray source emits monochromatic radiation:

$$\mathrm{y}_i = \int s_i(\mathrm{E}) \exp\left(- \oint_i \rho(x,y,z,\mathrm{E}) \mathrm{d}l \right) \mathrm{d}E \tag{1}$$

$$\simeq s_i(\mathrm{E}_0) \exp\left(- \oint_i \rho_0(x,y,z) \mathrm{d}l \right), \tag{2}$$

where $s(E)$ denotes the incident X-ray spectrum, $\rho(\cdot)$ stands for an attenuation coefficient, and $\oint_i(\cdot)\mathrm{d}l$ is the line integral between the source and the i-th detector pixel. It leads to a more manageable model solely comprised of the line integral, compared to (1) in which two integrals are coupled. Due to the ignorance of energy dependency, however, image degradations such as beam hardening artifact often occur.

To find the exact solution of (1), the polychromatic nature of CT data should be considered [1, 2]. In this paper, we newly employ the generalized information theoretic discrepancy (GID) as the data-mismatch term in the objective function, and propose information theoretic discrepancy based iterative reconstructions (IDIR). Similar to Csiszar's I-divergence [3], the GID between two nonnegative functions is defined as follows:

$$\mathcal{G}(\mathrm{y}||\hat{\mathrm{y}}) = \sum_i \mathrm{y}_i \cdot \varphi\left(\frac{\mathrm{y}_i}{\hat{\mathrm{y}}_i} \right), \tag{3}$$

where $\varphi(\cdot)$ is a convex function with the minimum at 1. The "distance" in (3) is closely related to the ratio between two variables. By using this particular feature, the GID of energy-integrated variables is transformed into that of imaginary variables reflecting the energy dependency. Two associated integrals in (1) are decoupled in the derived objective function, which leads to a tractable optimization problem even without the monochromatic approximation.

There are two possible data types for formulating the GID: the raw intensity measurement of detector and its log-transformed value. The statistical reconstruction prefers the former type, whereas the algebraic reconstruction is usually calculated after log-transform. We consider both data types, and then present corresponding two IDIR algorithms.

In preliminary experiments with a simulated dual energy CT and a real experimental tomosynthesis, the proposed algorithm shows superior performances over conventional reconstruction methods.

*Contact author: ke.jang@samsung.com

2. THEORY

2.1. IDIR: Raw Domain Version

Assume that an object $\mathbf{x}$ to be reconstructed consists of K-materials. Let $\hat{\mathrm{x}}^{(k)}$ be the current estimates of the k-th component substance. Let $\hat{\mathrm{p}}_i^{(k)}$ denote the result of the line integral of $\hat{\mathrm{x}}^{(k)}$ along the X-ray source and the i-th detector pixel, namely, "projection":

$$\hat{\mathrm{p}}_i^{(k)} = \sum_j a_{i,j} \cdot \hat{\mathrm{x}}_j^{(k)},$$

where j is the voxel index. According to (1), the simulated data $\hat{\mathrm{y}}_i$ is given by

$$\hat{\mathrm{y}}_i = \sum_E m_i(E), \quad m_i(E) = s_i(E) \exp(-\boldsymbol{\mu}(E)^T \hat{\mathbf{p}}_i), \quad (4)$$

where $\boldsymbol{\mu}(E) = [\mu^{(1)}(\cdot), \cdots, \mu^{(K)}(\cdot)]^T$, $\hat{\mathbf{p}}_i = [\hat{\mathrm{p}}_i^{(1)}, \cdots, \hat{\mathrm{p}}_i^{(K)}]^T$.

Since two integrals – the line integral along the pathway of X-ray photons and the energy integral – are coupled as in (4), it is difficult to incorporate the spectral information into the reconstruction procedure. To find the exact solution of (4), the GID in (3) is newly employed as the data-mismatch term. Then, we derive the following equivalence:

$$\begin{aligned} \mathrm{y}_i \cdot \varphi\left(\frac{\mathrm{y}_i}{\hat{\mathrm{y}}_i}\right) &= \left(\frac{\mathrm{y}_i}{\hat{\mathrm{y}}_i}\right) \hat{\mathrm{y}}_i \cdot \varphi\left(\frac{\mathrm{y}_i}{\hat{\mathrm{y}}_i}\right) \\ &= \sum_E \left(\frac{\mathrm{y}_i}{\hat{\mathrm{y}}_i}\, m_i(E)\right) \cdot \varphi\left(\frac{\mathrm{y}_i}{\hat{\mathrm{y}}_i} \cdot \frac{m_i(E)}{m_i(E)}\right) \\ &= \sum_E d(E) \varphi\left(\frac{d(E)}{m(E)}\right), \end{aligned} \quad (5)$$

where $m(E)$ is the monochromatic model at the E-th energy bin and $d(E)$ is the ratio between y and $\hat{\mathrm{y}}$ weighted by $m(E)$. It indicates that the GID of energy-integrated variables is equivalent to that of imaginary variables defined in each energy bin. Note that similar equivalence for $\varphi(u) = \log(u) + 1/u + 1$ was shown in [2].

The proposed method interprets that two variables $m(E)$ and $d(E)$ are independent each other, and use the alternating minimization scheme [2]. Since $d(E)$ can be automatically determined by (5), we only consider the update of $m(E)$ for given $\hat{d}(E)$. The effective data fidelity terms, $c_i(\cdot)$'s, are given as follows:

$$\sum_{i,E} c_i(\mathbf{p}_i, E) = \sum_{i,E} \hat{d}(E) \varphi\left(\frac{\hat{d}(E)}{m(E)}\right). \quad (6)$$

Note that $c_i(\cdot)$ is convex with respect to $\mathbf{p}_i$ for some $\varphi(\cdot)$'s.

To solve (6), we use the optimization transfer principle [4]. The object $\mathbf{x}$ is then estimated by iteratively minimizing a paraboloidal surrogate function $q_i(\cdot)$ which is given by

$$\begin{aligned} q_i^\epsilon(\mathbf{p}_i) &= \sum_E c_i(\hat{\mathbf{p}}_i, E) + \mathrm{g}_i(\hat{\mathbf{p}}_i, E)^T \mathbf{u}_i + \frac{1}{2} \mathbf{u}_i^T \mathrm{H}_i(\hat{\mathbf{p}}_i, E) \mathbf{u}_i \\ &= c_i^\epsilon(\hat{\mathbf{p}}_i) + \mathrm{g}_i^\epsilon(\hat{\mathbf{p}}_i)^T \mathbf{u}_i + \frac{1}{2} \mathbf{u}_i^T \mathrm{H}_i^\epsilon(\hat{\mathbf{p}}_i) \mathbf{u}_i, \end{aligned} \quad (7)$$

where $\mathbf{u}_i = \mathbf{p}_i - \hat{\mathbf{p}}_i$, and the superscript ϵ over a variable f, $f^\epsilon(\cdot)$, denotes the marginal sum over the energy variable E. In (7), $\mathbf{u}_i$ is the "non-constant" variable only related to $\mathbf{x}$, and thus two associated integrals in (1) are decoupled in the surrogate objective function.

When $\mathrm{g}_i^\epsilon(\cdot)$ and $\mathrm{H}_i^\epsilon(\cdot)$ satisfy monotonicity conditions as in [4], one may derive an algorithm guaranteeing the decrease of the objective value after each iteration. In this paper, the quadratic approximation to $c_i(\cdot)$ in (6) is used as the surrogate function. For twice continuously differentiable $\varphi(\cdot)$, $\mathrm{g}_i^\epsilon(\cdot)$ and $\mathrm{H}_i^\epsilon(\cdot)$ are given as follows:

$$\begin{aligned} \mathrm{g}_i^\epsilon(\hat{\mathbf{p}}_i) &= e_i^2 \varphi'(e_i) \sum_E \hat{m}_i(E) \boldsymbol{\mu}(E) \\ \mathrm{H}_i^\epsilon(\hat{\mathbf{p}}_i) &= (e_i^3 \varphi''(e_i) + e_i^2 \varphi'(e_i)) \sum_E \hat{m}_i(E) \boldsymbol{U}(E), \end{aligned}$$

where $\boldsymbol{U}(E) = \boldsymbol{\mu}(E) \boldsymbol{\mu}(E)^T$.

The structure of (7) is identical with that of the cost function with the monochromatic approximation (2), which solely consists of the line integral. We can use, therefore, the conventional methods for solving (7). Among various methods, we take the simultaneous update approach that allows an accelerated implementation using parallel computing. To achieve the concurrent updates of all voxels, we derive the separable surrogate function (SSF) [4], which directly relates the objective value to individual voxel $\mathbf{x}_j$. Since $\mathrm{q}_i^\epsilon(\cdot)$ in (7) is convex, the following inequality holds for $\sum_j \alpha_{i,j} = 1$, $\alpha_{i,j} \geq 0$:

$$\sum_i q_i^\epsilon(\mathbf{p}_i; \hat{\mathbf{p}}_i) \leq \sum_{i,j} \alpha_{i,j} q_i^\epsilon \left(\frac{a_{i,j}}{\alpha_{i,j}} (\mathbf{x}_j - \hat{\mathbf{x}}_j) + \hat{\mathbf{p}}_i; \hat{\mathbf{p}}_i \right),$$

which is called De Pierro's convexity technique [4]. By using the Newton-Raphson method, the final updating equation is given as follows:

$$\mathbf{x}_j = \hat{\mathbf{x}}_j - \left(\sum_i a_{i,j} \gamma_i \mathrm{H}_i^\varepsilon(\hat{\mathbf{p}}_i) \right)^{-1} \left(\sum_i a_{i,j} \mathrm{g}_i^\varepsilon(\hat{\mathbf{p}}_i) \right), \quad (8)$$

where $\gamma_i = \sum_j a_{i,j}$ [4].

2.2. IDIR: Log Domain Version

In algebraic reconstruction, the data-mismatch term is usually defined in log domain. It might be more appealing than raw domain approach, since the discrepancies for highly attenuated data are heavily weighted compared with those in raw

domain. Let $\hat{z}_i$ denote $(-\log \hat{y}_i)$. We introduce the new two constants $\mathcal{E}_i$ and B_i for the GID between the actual data z and $\hat{z}$ as follows:

$$\mathcal{G}(z||\hat{z}) = \sum_i (z_i + \mathcal{E}_i + B_i) \cdot \varphi\left(\frac{z_i + \mathcal{E}_i}{\hat{z}_i + \mathcal{E}_i}\right). \quad (9)$$

During the iterations of IDIR over log domain, a negative value of $\hat{z}$ can be appeared, since it is difficult to incorporate the positivity constraint, $\mathbf{x} > 0$, to the simultaneous update scheme. The constant $\mathcal{E}_i$ ensures that $(\hat{z}_i + \mathcal{E}_i)$ is always greater than 0. The constant B_i penalizes the discrepancy in the background region.

Since $-\log(u)$ is convex for $u > 0$, the following inequality holds for $\sum s_i(E) = 1$:

$$\begin{aligned}\hat{z}_i + \mathcal{E}_i &\le \sum_E s_i(E)\left(-\log\left(\exp(-\boldsymbol{\mu}(E)^T\hat{\mathbf{p}}_i)\right)\right) + \mathcal{E}_i \\ &= \sum_E s_i(E)\boldsymbol{\mu}(E)^T\hat{\mathbf{p}}_i + \epsilon_i(E) = \sum_E t_i(E), \quad (10)\end{aligned}$$

where $t_i(E)$ is an imaginary variable similar to $m(E)$ in (4), and $\epsilon_i(\cdot)$ is an arbitrary nonnegative function that satisfies $\sum \epsilon_i(E) = \mathcal{E}_i$. In a similar manner to (5), we can derive a surrogate GID defined in each energy bin E:

$$\begin{aligned}\mathcal{G}(z_i||\hat{z}_i) &\le \sum_E \left(\frac{z_i + \mathcal{E}_i}{\hat{z}_i + \mathcal{E}_i} t_i(E) + b_i(E)\right) \varphi\left(\frac{z_i + \mathcal{E}_i}{\hat{z}_i + \mathcal{E}_i}\frac{t_i(E)}{t_i(E)}\right) \\ &= \sum_E (d_i^{\mathrm{L}}(E) + b_i(E)) \varphi\left(\frac{d_i^{\mathrm{L}}(E)}{t_i(E)}\right), \quad (11)\end{aligned}$$

where the marginal sum of $b_i(\cdot)$ is equal to B_i.

Using the close resemblance between (5) and (11), the log domain version can be derived as in the previous section. The update equation is similar to (8), except the coefficients of the surrogate function:

$$\begin{aligned}g_i^{\epsilon}(\cdot) &= -e_i\varphi'(e_i)\sum_E s_i(E)\boldsymbol{\mu}(E)\left(e + \frac{b_i(E)}{t_i(E)}\right), \\ H_i^{\epsilon}(\cdot) &= \left(2e_i\varphi'(e_i) + e_i^2\varphi''(e_i)\right)\sum_E \frac{s_i^2(E)\boldsymbol{U}(E)}{t_i(E)}\left(e + \frac{b_i(E)}{t_i(E)}\right).\end{aligned}$$

3. RESULT

3.1. Implementation issues

In following experiments, $\varphi(u) = \sqrt{u} + 1/(4u^2)$. For accelerating the convergence speed, we use the ordered subset (OS) technique [4] and the multistep accelerated gradient method [5]. To avoid noise amplification, the total variation regularization is used [6].

3.2. Material decomposition in DECT

In the dual energy computed tomography (DECT), two sets of projections are obtained from distinct X-ray spectra. The material decomposition (MD) can be achieved by using the energy diversity of sinograms [7]. However, the MD is still challenging, since those two data sets are not spatially aligned in practice [8].



(a) Soft tissue (b) Bone

Fig. 1. Numerical phantom for simulation study.

A numerical phantom having the soft tissue and bone is illustrated in Fig. 1, which was generated from the segmented images of inner organs of the Visible Human Male [9] (VOXEL-MAN Group, University Medical Center Hamburg-Eppendorf). Two simulated polychromatic spectra with tube voltages of 70kV and 120kV were used. Based on the fan-beam geometry, each set of sinograms was calculated for 768 source locations over 360-degree. Two sets of projections were slightly misaligned by 0.2344-degree to simulate an alternating exposure of single X-ray source.

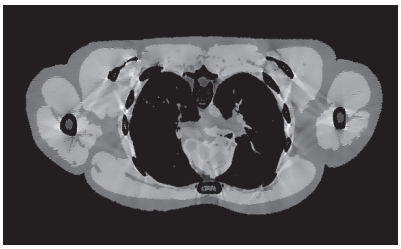
For comparison, an image-based material separation method [8] was implemented. In this approach, the MD is a weighted sum of two distinct reconstructed volumes that correspond to two sets of sinogram [8]. As shown in Fig. 2(a), the accuracy is limited due to the monochromatic approximation in the reconstruction stage.

The result of proposed algorithm is illustrated in Fig. 2(b). The IDIR over the log domain, performed 20 iterations with the OS acceleration. Compared to Fig. 2(a), beam hardening artifacts are considerably reduced. In addition, a superior resolution is achieved, since all sinograms were simultaneously utilized for reconstruction.

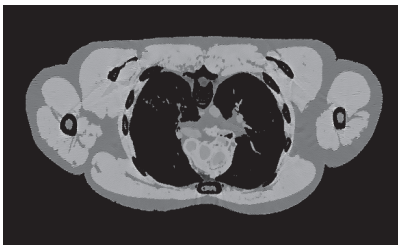
3.3. A wide angle DBT with voltage modulation

In the digital breast tomosynthesis (DBT), several low-dose projections are measured over a limited angle range. In general, a wider angular coverage might be desired for reducing the interplane blurring. For the oblique part of the source trajectory, however, measurements may be degraded by Poisson noise, due to the lack of penetrating power of X-ray beam. The voltage modulation may resolve this problem by using a high energy spectrum with large penetrating power for outlying frames.

An experimental DBT system was constructed using a tungsten anode X-ray tube (Varian Medical Systems, USA) and a full field digital X-ray detector (Dexela, UK). Under the approval of institutional review board of Samsung Medical Center (Seoul, Korea), two mastectomy specimens were examined. Several numerical lesions were added into measured sinograms.

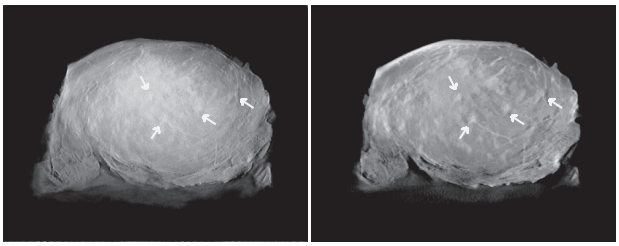


(a) Conventional image-based method

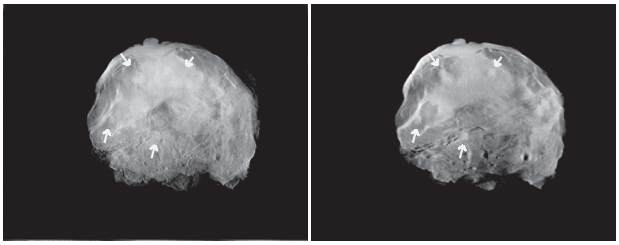


(b) Log domain version of IDIR algorithm

Fig. 2. Soft-tissue separation in the numerical DECT.



(a) Case 1, Narrow (b) Case 1, Wide



(c) Case 2, Narrow (d) Case 2, Wide

Fig. 3. Results with the experimental DBT equipment. (a) and (c): Narrow angle. (b) and (d): Wide angle with the voltage modulation, reconstructed by raw domain IDIR algorithm.

We present reconstructed slices over a narrow angular range of 15° in Fig. 3(a)(c). In Fig. 3(b)(d), those over 100°-angular range are illustrated. 20 iterations of the raw domain version of IDIR algorithm were used with the multi-step accelerated gradient method. The wide angle DBT was successfully implemented by employing the voltage modulation. Even though the spectral inhomogeneity presents in measured sinograms, beam hardening artifacts were hardly observed in reconstructed slices. Due to the improved depth-directional resolution, we can clearly observe lesions from Fig. 3(b)(d).

4. CONCLUSION

In this paper, the IDIR algorithm is proposed to account the exact polychromatic model. On the basis of new GID measure, a surrogate function with the decoupled integral is derived, thereby leading to a tractable optimization problem without the monochromatic approximation. In preliminary studies with the simulated DECT and the real experimental DBT, the proposed reconstruction algorithm showed the superior performances over conventional methods.

5. REFERENCES

[1] I.A. Elbakri and J.A. Fessler, "Statistical image reconstruction for polyenergetic x-ray computed tomography," *IEEE Trans. Med. Imag.*, vol. 21, no. 2, pp. 89–99, 2002.

[2] J.A. O'Sullivan and J. Benac, "Alternating minimization algorithms for transmission tomography," *IEEE Trans. Med. Imag.*, vol. 26, no. 3, pp. 283–297, 2007.

[3] I. Csiszar, "I-divergence geometry of probability distributions and minimization problems," *Ann. Probab.*, pp. 146–158, 1975.

[4] H. Erdogan and J.A. Fessler, "Ordered subsets algorithms for transmission tomography," *Phys. Med. Biol.*, vol. 44, pp. 2835–2851, 1999.

[5] A. Beck and M. Teboulle, "A fast iterative shrinkage-thresholding algorithm for linear inverse problems," *SIAM J. Imag. Sci.*, vol. 2, no. 1, pp. 183–202, 2009.

[6] K.E. Jang, Y. Sung, K. Lee, J. Lee, and S. Cho, "Statistical reconstruction using dual formulation of subband-wise total variation regularization (SDST) for limited angle tomography," in *IEEE Int. Symp. Biomed. Imag.*, 2011, pp. 1762–1765.

[7] R.E. Alvarez and A. Macovski, "Energy-selective reconstructions in x-ray computerised tomography," *Phys. Med. Biol.*, vol. 21, pp. 733, 1976.

[8] R. A. Brooks, "A quantitative theory of the hounsfield unit and its application to dual energy scanning," *J. Comput. Assist. Tomo.*, vol. 1, no. 4, pp. 487–493, 1977.

[9] K.H. Höhne, B. Pflesser, A. Pommert, M. Riemer, R. Schubert, T. Schiemann, U. Tiede, and U. Schumacher, "A realistic model of human structure from the visible human data," *Method Inform. Med.*, vol. 40, no. 2, pp. 83–89, 2001.